JMEPEG (2023) 32:9163–9173
https://doi.org/10.1007/s11665-023-08080-4

1059-9495/$19.00

TECHNICAL ARTICLE

Electrochemical Investigations on the Corrosion Behavior of 904L Stainless Steel in LiBr Solutions

Sherief A. Al Kiey, E.A. Abd El Meguid, and S.S. Abd El Rehim

Submitted: 5 April 2022 / Revised: 27 December 2022 / Accepted: 27 January 2023 / Published online: 3 April 2023

The pitting corrosion susceptibility of 904L stainless steel in aerated LiBr solutions was investigated. The influence of various experimental variables, including electrolyte concentrations, pH, scan rate, temperatures, and constant potential has been studied using electrochemical measurements, such as cyclic potentiodynamic polarization, potentiostatic techniques, and electrochemical impedance spectroscopy (EIS). The surface morphology of 904L stainless steel was examined by scanning electron microscope (SEM). The rate of uniform corrosion and susceptibility toward pitting corrosion increases with an increase in LiBr concentrations and temperature. Increasing the pH of the solution decreases the rate of both uniform and pitting corrosion. An increase in the scan rate enhances the uniform corrosion, but suppresses the pitting corrosion. EIS diagrams displayed a depressed semicircles with the center under the real axis. Bode plots support the result that the uniform corrosion resistance of the alloy in LiBr solutions decreases with increasing Br^- anion concentration. The observations suggest that this one time constant may actually be the overlap of two-time constants.

Keywords cyclic polarization, EIS, passivity, pitting corrosion, superalloys

1. Introduction

Lithium bromide (LiBr) has extensively been utilized as an absorption working fluid in absorption refrigeration units because of the pressure decrease that occurs when water steam is absorbed by lithium bromide. It is one of the superior choice fluids found among different fluids (Ref 1). LiBr possesses favorable thermophysical characteristics (i.e., high hydration heat, good thermal stability, and low viscosity) and it does not present any crystallization problems in the structural materials of the refrigeration system (Ref 2-6). It has many advantages such as energy-saving and deucing the problems of the environmental effects of chlorofluorocarbons (CFCs) and hydrochlorofluorocarbons (HCFCs) (Ref 7). Although LiBr solutions have excellent properties and are the preferred option used in many applications, they are corrosive to many metals, and attack the material of the equipment throughout the operating conditions due to the presence of certain aggressive anions, and bromides (Br^-). Therefore, many corrosion problems such as pitting and general corrosion (Ref 6, 8-10) generate inside the refrigeration unit and decrease the operating efficiency.

Sherief A. Al Kiey and **E.A. Abd El Meguid**, Physical Chemistry Department, National Research Centre, Dokki, Egypt; and **S.S. Abd El Rehim**, Chemistry Department, Faculty of Science, Ain Shams University, Cairo, Egypt. Contact e-mail: sheriefalkiey@yahoo.com.

Pitting corrosion of metals and alloys is the main reason for failure in many industrial media. Consequently, it is important to study the pitting corrosion behavior in LiBr solutions. One of the methods to solve this corrosion problem is developing new engineering alloys that have high corrosion resistance, low cost, and superior technological performance. Due to their high mechanical strength and resistance to corrosion, austenitic stainless steels have been used extensively in industrial applications, such as heat exchangers and chemical industries (Ref 11-14). They are regularly employed as structural components in absorption machines. 904L austenitic stainless steel (904L) is a super austenitic stainless steel designed for use in more aggressive conditions and to provide long-term corrosion performance (Ref 15-18). Due to the formation of a dense passive layer on the steel surface, 904L austenitic stainless steel provides unique resistance to pitting corrosion (Ref 19-21), crevice corrosion (Ref 22), erosion corrosion (Ref 23), and stress corrosion cracking (Ref 24, 25). It also contains significant amounts of Cr and Ni with additional Mo and Cu (Ref 26-28). Other elements, such as Mo and N, also significantly boost corrosion resistance in aggressive environments. This is most likely due to the two components' synergistic impact (Ref 29-31). The outstanding corrosion resistance of stainless steel is owing to the spontaneous formation of a protective passive layer with a thickness of a few nanometers (nm) on the surface. This film is composed of an oxide film that protects the steel from attack in an aggressive environment (Ref 32, 33).

One of the methods to solve this corrosion problem is developing new engineering alloys that have high corrosion resistance, low cost, and superior technological performance. Due to their high mechanical strength and resistance to corrosion, austenitic stainless steels have been used extensively in industrial applications, such as heat exchangers and chemical industries.

The objective of the present work is studying the pitting corrosion behavior of high mechanical strength and resistance to corrosion 904L Stainless Steel in LiBr solutions that has

been employed in absorption refrigeration systems under different experimental conditions such as bromide ion concentration, pH and temperatures employing electrochemical measurements as potentiodynamic cyclic polarization technique, potentiostatic measurements, and electrochemical impedance spectroscopy (EIS) technique and complemented by SEM.

2. Experimental Procedure

904L stainless steel alloy (Avesta AB (Sweden)) was used in this study with the following chemical composition (wt. %): 19 Cr, 23 Ni, 4.5 Mo, 0.02 C, 0.195 N, the balance is Fe which was determined by the optical emission spectrometer. The working electrode was cut flags of 0.1 mm × 0.1 mm for electrochemical measurements. Prior to each experiment, the working electrode was mechanically polished electrode with different emery papers up to 1000 grade to ensure the same surface roughness, rinsing with ethanol and drying in the air. The edges and backs of electrodes were coated with a high strength epoxy resin (Araldite), leaving 10 × 10 mm surface area to avoid crevice effects. A conventional electrochemical cell was used containing three compartments for working, platinum counter and saturated calomel reference electrodes. The experimental techniques used in the present investigation are cyclic potentiodynamic, potentiostatic and electrochemical impedance measurements. The measurements were carried out in aerated LiBr solutions at the required temperature (± 1 °C), using a water thermostat. All solutions were freshly prepared from analytical grade chemical reagents using doubly distilled water without further purification.

All electrochemical measurements were carried out using the electrochemical workstation Voltalab 40, France. Cyclic potentiodynamic polarization studies were conducted at a scanning rate of 5 mV/s from − 700 to + 700 mV with respect to the open circuit potential (OCP) of the 904L stainless steel. Then the scan direction was reversed at − 700 mV at the same scan rate until forming a complete cycle. Both of E_{pit} and E_{prot} were determined from potentiodynamic polarization curves as the potentials at which the current density exceeds 100 μA cm^{-2} in the forward scan and goes below to 100 μA cm^{-2} in the reverse scan, respectively. All electrode potentials were measured referring to the saturated calomel electrode (SCE). The electrochemical parameters, corrosion current density (i_{corr}), corrosion potential (E_{corr}), and Tafel anodic and cathodic slopes (β_a, β_c) were extracted from the extrapolation of Tafel lines. To study the effect of temperature, the cell was immersed in water thermostat in the temperature range from 25, 40, 50, 60, and 70 ± 1 °C. Chronoamperometric measurements (current- time) were carried out adjusting the electrode at constant step potential where the current was recorded as a function of time. Impedance studies were conducted with AC signal amplitude of 10 mV peak to peak in a frequency domain from 0.1 Hz to 100 kHz. The EIS was recorded after reading a steady state open-circuit potential. The surface morphology of 904L stainless steel specimen was characterized by the scanning electron microscope (JEOL-JEM-100 s).

3. Results and Discussion

3.1 Cyclic Potentiodynamic Polarization

Cyclic potentiodynamic polarization curves of 904L stainless steel in different concentrations (0.01–2 M) of aerated LiBr solutions were recorded at 25 °C at pH of 8.6. In all solutions, the curves were recorded starting from -700 mV toward more positive potential values with a scan rate of 5 mV/s up to 700 mV$_{(SCE)}$. For simplicity, Fig. 1 represents some examples of these curves. Similar curves were recorded in other concentrations.

The results showed in all solutions tested and under the present experimental conditions, the reduction of oxygen represents the most probable partial cathodic reaction according to equation (Ref 34):

$$O_2 + 2H_2O + 4e^- \rightarrow 4OH^- \quad \text{(Eq 1)}$$

As this reaction proceeds, local sites of alkalinity are established which leads to the formation of defective and a porous oxide film on the electrode surface (Ref 35). This reaction enhances with increasing LiBr concentration (Ref 36-38). Therefore, around the corrosion potential zone, the alloy exhibits high corrosion resistance and spontaneous passivity. This passivity is due to the presence of defective iron oxide film containing Cr_2O_3-based products on the surface of 904L stainless steel in this medium (Ref 39-42). Therefore, this zone is characterized by the observation of oscillations in current. These oscillations were also observed for stainless steel in LiBr media (Ref 43). The appearance of current oscillations is indicative of the formation of metastable pitting corrosion as a result of consecutive formation and repassivation of microsize pits (Ref 44-46). These metastable pits grow and repassivate quickly. It is seen that the oscillation phenomenon decreases and the value of current density slightly increases with increasing the anodic potential up to a certain critical potential (breakdown potential E_{pit}), which is an indication of local loss of passivity or local film breakdown, at which the passive current density (J_{pass}) rises sharply and rapidly without any sign of oxygen evolution indicating initiation and propagation of stable pits (Ref 47). Finally, this rising pitting current density (J_{pit}) tends to achieve a steady state value with further increase in the anodic potential. The value of E_{pit} could be taken as a measure of tendency of metal and alloys to undergo stable pitting corrosion in a certain environment.

Initiation of pitting could be explained using the point defect model (PDM) previously published (Ref 48-50). According to this model, the adsorbed Br^- anions on the anode surface incorporate the passive oxide film by occupying the anion vacancies. This leads to a decrease in the anion vacancies and increases in the cation vacancies. When the cation vacancies start to pile up at the metal interface, a breakdown of the passive film takes place. Propagation and growth of pitting corrosion results from changes in the solution chemistry inside the pits. The solution inside pits becomes more aggressive and more acidic as a result of the migration of Br^- ions into the pits and the hydrolysis of corrosion products inside pits (Ref 51).

It is obvious from cyclic polarization curves that upon reversing the forward potential scan a current hysteresis loop appears, so that the alloy is able to repassivate after the breakdown of the passive film. Repassivation takes place at a certain potential known as repassivation or protection potential (E_{prot}). It is the potential where the forward and the reverse curve crosses. E_{prot} value is taken as the lowest potential above which the already initiated pit can grow while below it no pit can initiate. The larger the hysteresis loop, the more difficult it becomes to repassivate the pit (Ref 52).

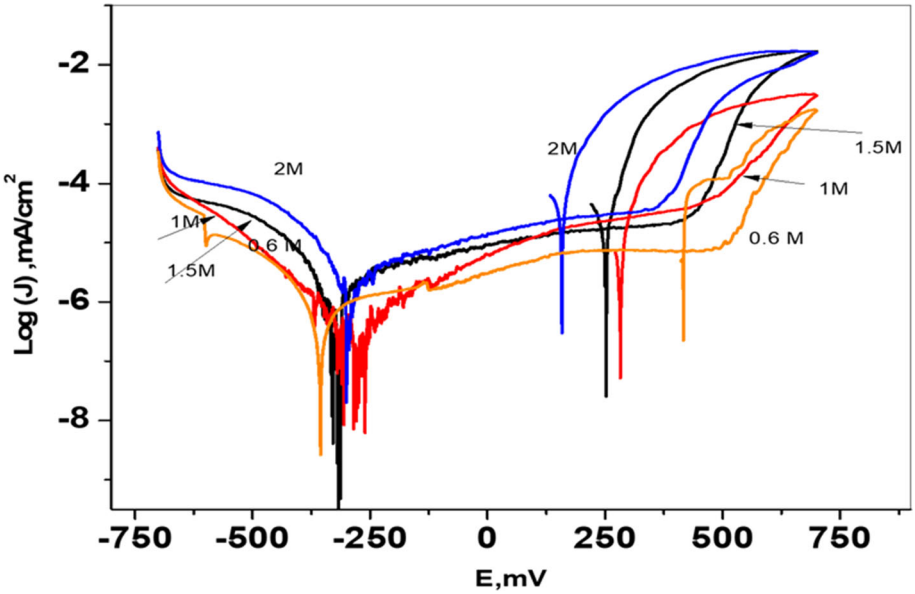

Fig. 1 Potentiodynamic cyclic polarization curves of 904L stainless steel in different concentrations of LiBr [M] at scan rates of 5 mV/s and 25 °C

Table 1 The electrochemical parameters obtained from potentiodynamic cyclic polarization curves for 904L stainless steel in different LiBr concentrations at 5 mV/s and 25 °C

Concentration, M	E corr, mV	J corr, A/cm$^2\mu$	E pit, mV	E prot, mV
0.01	− 327.1	0.003	868.0	629.5
0.1	− 360.8	0.255	609.2	583.0
0.3	− 382.6	0.645	604.0	392.2
0.5	− 361.5	1.126	606.0	424.2
0.6	− 355.4	1.240	559.4	420.0
1.0	− 368.4	1.850	530.5	305.4
1.5	− 328.7	4.821	499.1	284.0
2	− 299.0	5.041	428.0	629.5

The electrochemical parameters associated with cyclic polarization curves for 904L stainless steel in different concentrations of LiBr are listed in Table 1. Inspection of these parameters reveals that the uniform corrosion potential E_{corr} slightly shifts to more negative direction and corrosion current density J_{corr} increases with increased LiBr concentrations.

The relation between J_{corr} and LiBr concentrations is shown in Fig. 2. These results reveal that an increase in LiBr concentration enhances the rate of uniform (general) corrosion of 904L stainless steel in this medium. Moreover, an increase in the concentration of LiBr enhances the passive current density J_{pass}, decreases the pitting potential E_{pit} and increases the pitting current density J_{pit}. The relation between E_{pit} and the bromide concentration is illustrated in Fig. 2. It is clear that the less positive value of E_{pit}, the less resistant the alloy is to undergo pitting corrosion. The value of repassivation potential E_{prot} also shifts to less positive value with increasing LiBr concentration. The larger values of ΔE (i.e. $\Delta E = E_{pit} - E_{prot}$) indicate that the repassivation of stable pits becomes more difficult to increase the electrolyte concentration.

3.1.1 Effect of pH. The effect of increasing pH of the LiBr solution on both uniform and pitting corrosion of 904L stainless steel was investigated. Figure 3 illustrates the cyclic polarization curves of the alloy in 1 M LiBr at 25 °C and scan rate of 5 mV/s with two different pHs: 8.6 and 9.0. The higher pH was achieved by addition of LiOH drops into the blank solution.

The results reveal that an increase in pH of the blank solution from 8.6 to 9.0 inhibits the cathodic reduction reaction, but enhances the anodic oxidation processes especially at low anodic potentials. The corrosion potential E_{corr} shifts from − 368.4 mV at pH 8.6 to − 518.1 mV at pH 9.0. This shift could be due to the inhibition of the partial cathodic reduction reaction. The corrosion current density J_{corr} decreases from 1.850 to 1.055 μA cm^{-2} with increasing pH of the solution indicating a decrease in the uniform corrosion rate of the alloy. Moreover, it is found that as the pH of the solution increases, the pitting potential E_{pit} shifts from 530.5 to 577.1 mV indicating an increase in the pitting corrosion resistance. Therefore, it is evident from these data that an increase in pH from 8.6 to 9.0 of the bromide solutions inhibits both uniform and pitting corrosion of 904L stainless steel in 1 M LiBr.

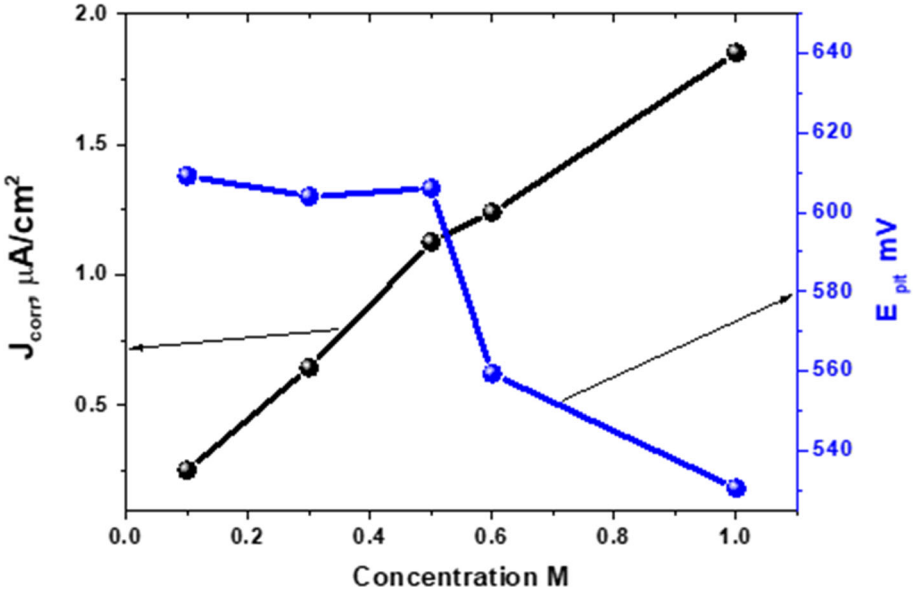

Fig. 2 The relation between LiBr concentration and corrosion current density and pitting potential E_{pit} at scan rate of 5 mV/s, 25 °C

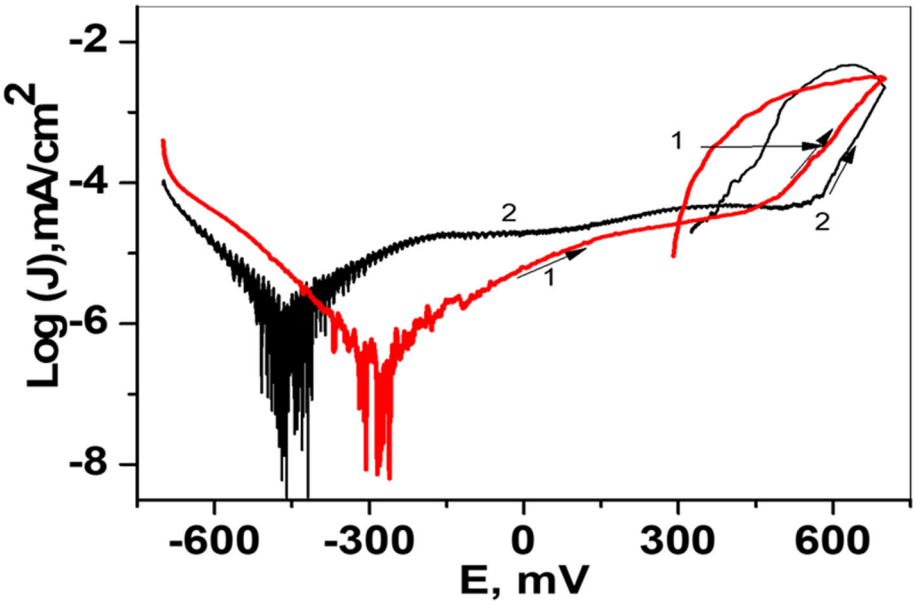

Fig. 3 Potentiodynamic cyclic polarization curves of 904L stainless steel at different pHs (a) 8.6 (b) 9.0 in 1 M LiBr at 25 °C and a scan rate of 5 mV/s

3.1.2 Effect of Temperature. The influence of temperature on both uniform and pitting corrosion of 904L stainless steel in aerated 1 M LiBr (pH = 8.6) solution was investigated. Figure 4 shows the cyclic polarization curves for904L stainless steel obtained at scan rate of 5 mV/s in 1 M LiBr solution at temperature range between 25 and 70 °C. The electrochemical parameters obtained from these polarization curves are collected in Table 2.

It is clear that the value of corrosion current density and hence rate of uniform corrosion enhances with increasing solution temperature. This result is due to the increase effect of temperature on both anodic and cathodic partial reactions as demonstrated from the polarization curves.

The breakdown potential E_{pit} shifts to more active less (positive potential) with temperature increasing, suggesting that the investigated alloy's pitting corrosion resistance decreases with increasing temperature, which is due to the increased rate of chemical and electrochemical reactions as temperatures rise. This impact of temperature on 904L stainless steel pitting corrosion appears to be analogous to that previously reported for halide pitting corrosion in stainless steel (Ref 53, 54). There are two reasons why pitting susceptibility of the investigated alloy decreases as solution temperature rises. First, the passive film's porosity increases with temperature, and this improvement is confirmed by the finding that aggressive ions are incorporated into the passive films. Second, the chemical composition and/or physical structure of the passive film are

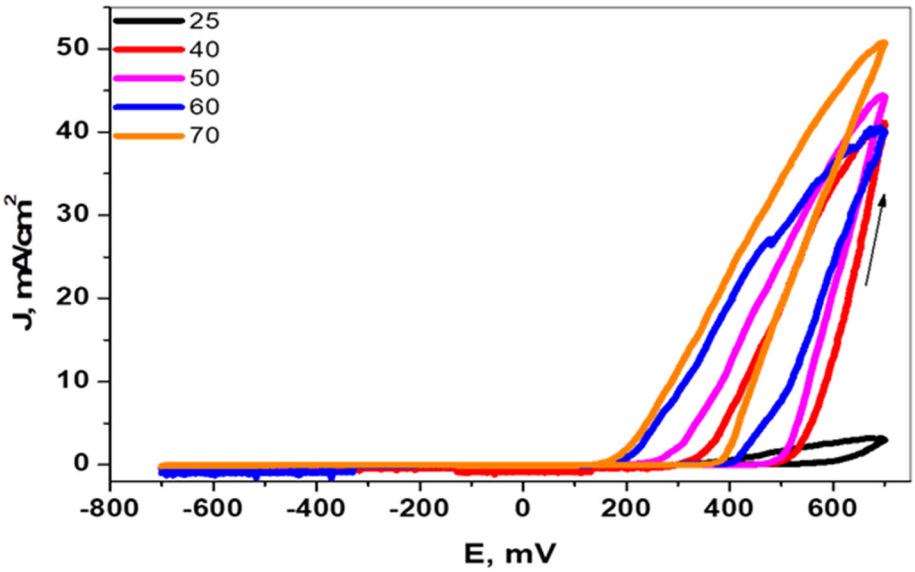

Fig. 4 Potentiodynamic cyclic polarization curves of 904L stainless steel at different temperatures in 1 M LiBr at scan rate of 5 mV/s

Table 2 The electrochemical parameters obtained from potentiodynamic cyclic polarization curves for 904L stainless steel in 1 M LiBr at different Temperatures

Temperature, C	E_{corr}, mV	J_{corr}, A/cm$^2\mu$	E_{pit}, mV	E_{prot}, mV
25	− 368.4	1.85	530.5	305.4
40	− 312.2	2.23	509.3	303.9
50	− 248.8	3.58	486.6	227.5
60	− 223.1	4.92	407.7	176.6
70	− 354.7	5.36	381.8	144.8

inherently changed (Ref 55). Manning claims that the passive oxide film's protective properties deteriorate with temperature and that the oxide coating on stainless steel changes from being p-type at normal temperature to n-type at higher temperatures (Ref 56).

3.2 Potentiostatic Polarization Measurement

In order to shed more light on pitting corrosion of 904L stainless steel electrode in aerated LiBr solutions, potentiostatic anodic polarization measurements (current–time transients) were performed under different experimental conditions, namely applied anodic potential, LiBr concentration and temperature. In addition the results give more information regarding the kinetics of passivity and passivity breakdown of 904L stainless steel electrode in LiBr solutions.

3.2.1 Effect of Potential. Figure 5 shows potentiostatic current/time transients for 904L stainless steel in 1 M LiBr at various applying anodic potentials (less and higher than E_{pit}) at 25 °C. It is obvious that at anodic potentials less positive than E_{pit}(300-500 mV), the very small passivation current density J_{pass} remains more or less constant but slightly increases with increasing the applied potential.

The passivation current density J_{pass} is related to the rate of electrochemical dissolution of the metal via the passive layer and chemical dissolution of the oxide by the adsorbed Br^- ions. At anodic potentials greater than E_{pit} (650-700 mV), the current tends to decline for a very short period before settling to a low value, defining the characteristic pitting parameter, namely the incubation time (t_i). The sample's susceptibility to pitting corrosion is reflected in the size of t_i. After t_i (i.e., after pit start), the pitting current density (J_{pit}) rapidly increases and eventually approaches a steady state. Passivity breakdown caused by aggressive Br- ions causes stable pits to form and propagate, resulting in a substantial increase in the passive current density (J_{pass}). The incubation time is found to decrease as the applied potential is increased.

Also, an increase in applied anodic potential enhances the electric field across the passive film and hence accelerates the adsorption of Br- ions on the passive surface (Ref 57). In addition, the pitting current density J_{pit} and its steady state increase with increasing the applied potentials. The steady state current density may be ascribed to a saturation concentration and precipitation of pitting corrosion products on the bottom of the pits and therefore, the dissolution process inside pits becomes under diffusion control (Ref 58). This limiting current density may be decreased with time especially at higher electrolyte concentrations.

3.2.2 Effect of LiBr Concentrations. Figure 6 displays current transients for 904L stainless steel in different concentrations of LiBr solutions (0.1–0.6 M) at applied anodic potential 580 mV ($> E_{pit}$) and at 25 °C. The data reveal that as the concentration of LiBr is increased, a very short

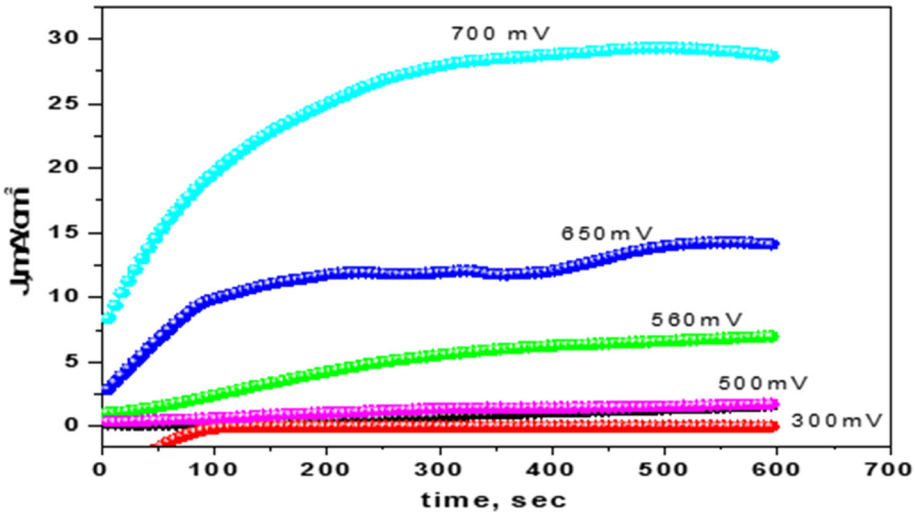

Fig. 5 Potentiostatic polarization (Current density versus time) curves for 904L stainless steel electrode in 1 M of LiBr at different anodic potentials at 25 °C

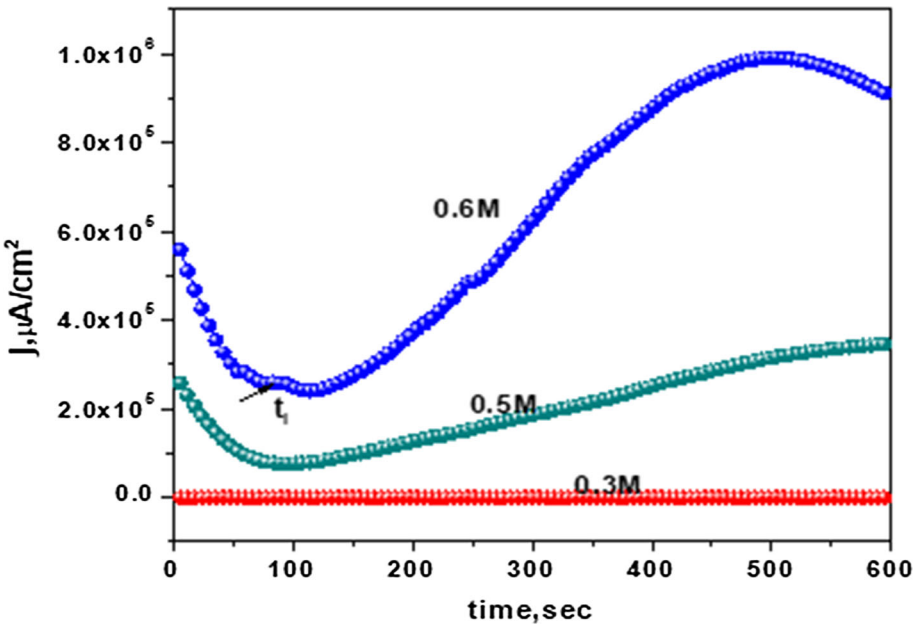

Fig. 6 Potentiostatic polarization (Current density versus time) at 580 mV_{SCE} for 904L stainless steel electrode in different concentrations of LiBr at 25 °C

incubation time and lager pitting current density J_{pit} are observed corresponding to an increase in the rate of pitting initiation and propagation.

3.2.3 Effect of Temperature. Figure 7 shows the influence of the temperature 25–70 °C on the feature of potentiostatic current transients for 904L stainless steel in 1 M LiBr at 580 mV ($> E_{pit}$). Inspection of the data reveals that incubation time t_i decreases and pitting corrosion current density J_{pit} increases with increasing temperature corresponding to an increase in the rate of pitting corrosion.

This trend could be explained as mentioned before to an increase in porosity of the passive film with temperature (Ref 55). Moreover, the chemical composition and/or physical structure of passive layer undergo modification with temperature (Ref 56). The increase in temperature promotes the rates of migration and diffusion of the reactant and product species to and from pits and therefore, increases the rate of pitting propagation. All these events facilitate the mission of the aggressive Br^- anion to destruct passivity of the oxide film, resulting in the occurrence of intense pitting corrosion. It is worth noting that all the potentiostatic current/time results support the potentiodynamic polarization results.

3.3 Electrochemical Impedance Measurements

Electrochemical impedance spectroscopy EIS is a powerful non-destructive technique that has been conducted to explain the corrosion and corrosion protection of metals and alloys in corrosive media (Ref 59, 60). Also, the EIS provides important

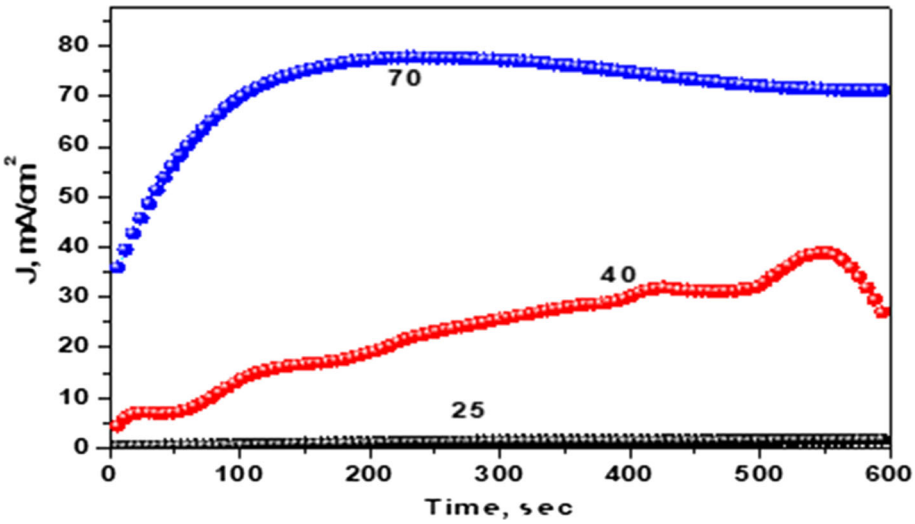

Fig. 7 Potentiostatic polarization curves (Current density vs. time) at 580 mV_{SCE} for 904L stainless steel electrode in 1 M LiBr at different temperatures

mechanistic and kinetic information for an electrochemical system under investigation. EIS measurements were performed to illustrate uniform corrosion of 904L stainless steel in aerated LiBr solutions at 25 °C. After 1 h of immersion, impedance spectra at open circuit potential are recorded. The impedance data recorded as Nyquist plots, Bode plots and phase angle diagrams as shown in Fig. 8. Usually, a mechanism of charge transfer on an inhomogeneous surface is interpreted by the Nyquist plots (Ref 61, 62). The EIS diagrams display typical behavior for a passive state, such as high impedance values with capacitive behavior that is consistent with the relevant literature (Ref 63). These capacitive loops are depressed semicircles with the center under the real axis. The depression is assigned to surface inhomogeneities resulting from surface roughness, defective and formation of porous oxide film covering the electrode surface (Ref 64).

The data reveal that the total impedance of the present system is high as a result of the existence of spontaneous oxide film exists on the alloy surface at OCP. The equivalent circuit model used for the present system is similar to that reported previously and is shown in Fig. 8d. This circuit consists of a solution resistance R_s in series with parallel combination of R_p and constant phase element CPE. The constant phase element is employed instead of a pure capacitance C_{dl} to fit the experimental impedance results. The fitted data are given in Table (3). This model assumes that the passive film does not completely cover the metal and therefore cannot be regarded as a homogeneous layer, but rather as a defective layer. Indeed, neither real surfaces of active materials nor passive films on metallic substrates may be regarded ideally homogenous (Ref 65). Constant phase element (CPE) is introduced to account for the non-ideal electric performance. A constant phase element (CPE) is used to describe a frequency independent phase change between alternating potential and its current response. Impedance representation defines CPE:

$$Z_{\mathrm{CPE}} = Y_0^{-1}(j\omega)^{-n} \qquad \text{(Eq 2)}$$

where Y_0 represents the CPE constant, ω is the angular frequency (in rad s^{-1}), and n represents the CPE exponent. The admittance and exponent n of the CPE are both independent of frequency (f), and all provide information regarding the degree of surface inhomogeneity. An imperfect capacitor would have a value of n less than unity, which is typically considered to come from a dispersion of relaxation times brought on by microscopic heterogeneities under the oxide phase and at the oxide/electrolyte interface (Ref 66).$\chi 2$ means the fitting error represents the deviation between experimental data and the fitted (less than 10^{-3}), indicating that the equivalent circuit model is applicable.

Regarding to Nyquist plots (Fig. 8a), it is clear that the diameter of these semicircles depends upon the concentration of LiBr. The resistance of oxide film R_p (the diameter of semicircle) and the capacity of electrical double layer C_{dl} which is equal (Ref 67).

$$f\left(-Z''_{\mathrm{img}}\right) = 1/\left(2\pi C_{dl} R_p\right) \qquad \text{(Eq 3)}$$

where Z''_{img} is the frequency at which the imaginary resistance components of the impedance is maximum were derived from Nyquist plots and are listed in Table 3.The data were analyzed using software provided with EIS 300 software. It is clear that the value R_p which is inversely proportional to the rate of uniform corrosion of the alloy decreases with increasing LiBr concentrations. These results agree well with those obtained from cyclic potentiodynamic polarization measurements.

Bode plots (Fig. 8b) displays high impedance values as a result of the existence of the spontaneous oxide film on the alloy surface at OCP. Bode plots do not involve a clear limiting DC resistive regions (horizontal lines) at low frequencies. These plots support the result that the uniform corrosion resistance of the alloy in LiBr solutions decreases with increasing Br^- anion concentration. One broad time constant is seen on the phase diagrams plots, as is immediately apparent in Fig. 8c. The observations suggest that this one time constant may actually be the overlap of two-time constants. This behavior is similar to that obtained as they obtained one depressed capacitive loop (one time constant in the Bode-phase representation) for the corrosion of duplex stainless steel in LiBr solutions (Ref 68).

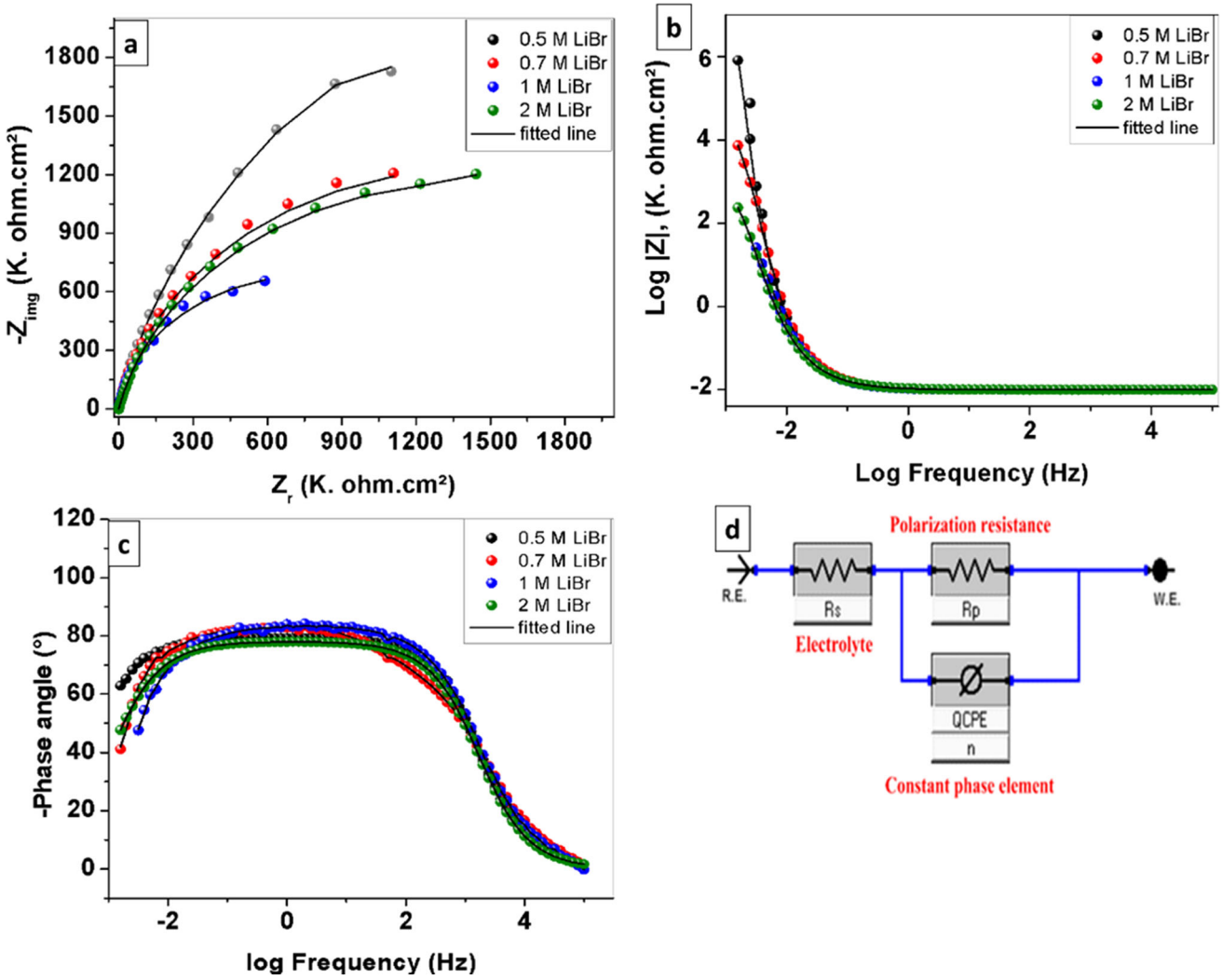

Fig. 8 (a) Nyquist plot (b, c) Bode and phase angle spectrum of 904L stainless steel electrode in solution containing different concentrations of LiBr at 25 °C (d) equivalent circuit utilized in fitting

Table 3 The electrochemical parameters for corrosion of 904L stainless steel electrode in solution containing different concentrations of LiBr at 25 °C (EIS)

			QCPE			
Concentration, M	**Rs, Ohm.cm^2**	**Rp, k.ohm.cm2**	**Y0$\mu\Omega$ − 1 sn cm − 2**	***n***	**CμF**	**χ2**
0.5	9.33	6.48	28.45	0.882	3.57	0.00409
0.7	9.30	2.91	28.14	0.894	4.07	0.0081
1.0	8.11	2.85	29.05	0.898	4.56	0.0079
2.0	5.81	1.56	31.01	0.918	6.89	0.0032

3.4 Surface Morphology

The scanning electron microscope SEM was used to investigate the surface morphology and confirm the occurrence of pitting corrosion of 904L stainless steel. Figure 9 illustrates SEM micrographs recorded for alloys immersed in LiBr solutions under potentiostatic regime for 10 min at anodic potential 500 mV ($< E_{pit}$) and at anodic potential 580 mV ($> E_{pit}$). It is observed that the surface morphologies depend on applied anodic potential, LiBr concentration and temperature. At anodic potential 500 mV the results show no evidence of pitting attack (Fig. 9a). However, passivity breakdown occurs and sever pitting attack appears in samples exposed to more noble potential than E_{pit} (at 580 mV). In all cases, the formed pits (or the pitted areas) are surrounded on all sides by regions covered with the oxide film. The pit area density increases with increasing the concentration of LiBr (Fig. 9b)

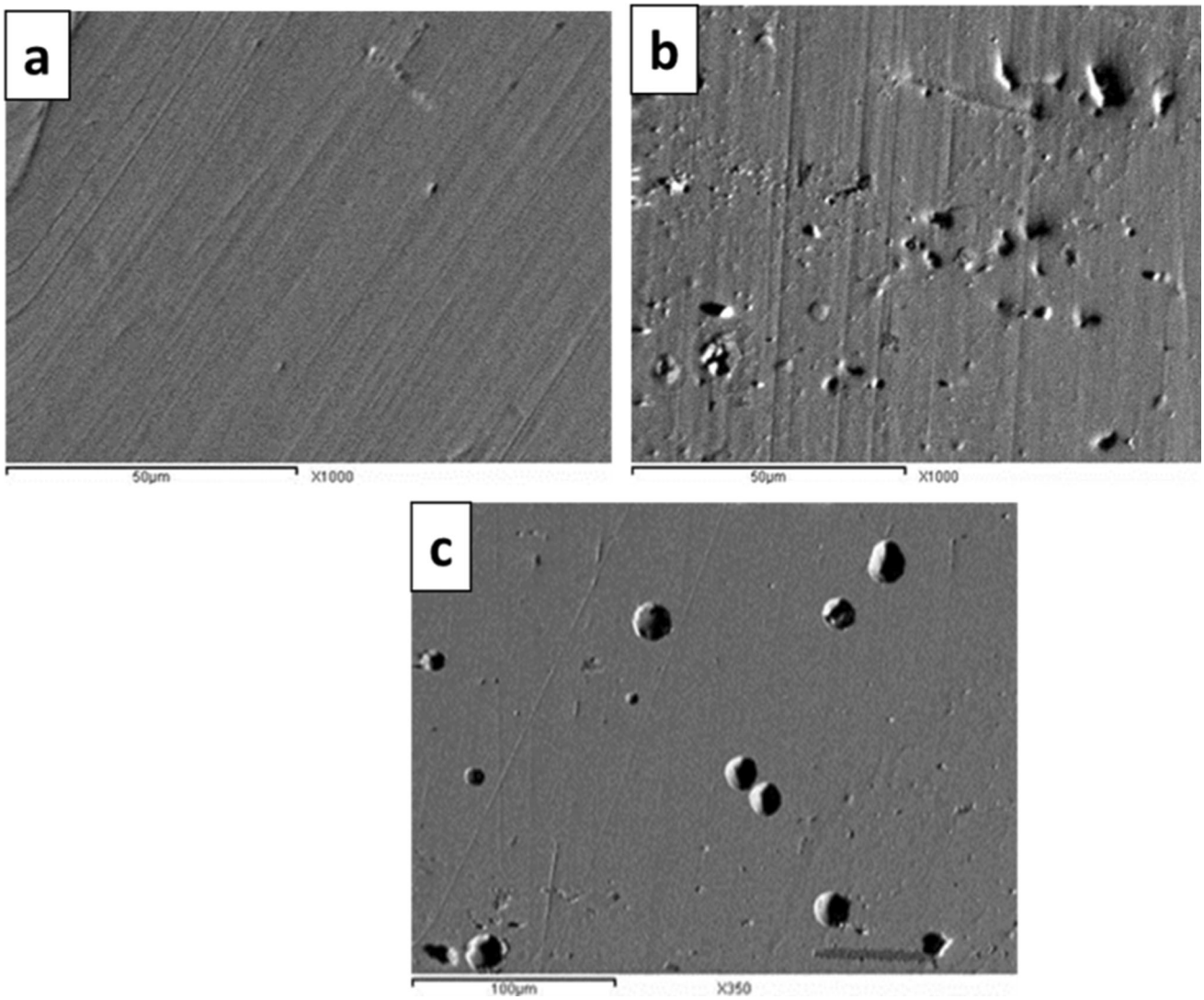

Fig. 9 Scanning electron microscopy (SEM) micrographs of 904L stainless steel surface after potentiostatic measurement for 10 min in (a) 500 mV, 25 °C (b) 580 mV,25 °C (c) 580 mV,70 °C

and with the temperature (Fig. 9c) corresponding to an increase in the susceptibility of pitting corrosion. These data support the potentiodynamic polarization measurements.

4. Conclusion

Cyclic potentiodynamic polarization, chronoamperometric and electrochemical impedance spectroscopy measurements were used to study the pitting corrosion behavior of 904L stainless steel in LiBr solutions. The obtained results show that the rate of uniform corrosion and susceptibility toward pitting corrosion increases with increasing LiBr concentrations and temperature. Increasing the pH of the solution decreases the rate of both uniform and pitting corrosion. An increase in the scan rate enhances the uniform corrosion, but suppresses the pitting corrosion. Nyquist plots displayed a depressed semicircles with the center under the real axis. Meanwhile, Bode plots support the result that the uniform corrosion resistance of the alloy in LiBr solutions decreases with increasing Br^- anion concentration. The results suggest that this one time constant may actually be the overlap of two-time constants. The surface morphology examination by scanning electron microscopy (SEM) confirmed the occurrence of pitting corrosion. The results obtained from EIS measurements are comparable with the data obtained from electrochemical measurements.

Acknowledgments

The authors thank the National Research Centre (NRC) for the technical and financial support.

Funding

Open access funding provided by The Science, Technology & Innovation Funding Authority (STDF) in cooperation with The Egyptian Knowledge Bank (EKB). This research did not receive any specific grant from any funding entities.

Data Availability

All data and materials are available.

Conflict of interest

The authors declare no conflict of interest.

Ethical Approval

Not applicable.

Open Access

References

1. P. Srikhirin, S. Aphornratana, and S. Chungpaibulpatana, A Review of Absorption Refrigeration Technologies, *Renew. Sustain. Energy Rev.*, 2001, **5**(4), p 343–372. https://doi.org/10.1016/S1364-0321(01)00003-X
2. K.E. Herold, R. Radermacher, and S.A. Klein, *Absorption Chillers and Heat Pumps*, CRC Press, London, 2016
3. D.-W. Sun, Thermodynamic Design Data and Optimum Design Maps for Absorption Refrigeration Systems, *Appl. Therm. Eng.*, 1997, **17**(3), p 211–221. https://doi.org/10.1016/S1359-4311(96)00041-5
4. J.L. Guiñon, J. Garcia-Anton, V. Pérez-Herranz, and G. Lacoste, Corrosion of Carbon Steels, Stainless Steels, and Titanium in Aqueous Lithium Bromide Solution. Corrosion, 1994, **50**(3), p 240–246. https://doi.org/10.5006/1.3293516
5. K.D. Rafferty, *Geothermal Direct Use Engineering and Design Guidebook, Geo-Heat Center*, Oregon Institute of Technology, Klamath Falls, 1991. https://doi.org/10.2172/5859999
6. A. Igual Munoz, J. García Antón, J.L. Guinón, and V. Pérez Herranz, Corrosion Behavior and Galvanic Coupling of Stainless Steels, Titanium, and Alloy 33 in Lithium Bromide Solutions, *Corrosion*, 2003, **59**(7), p 606–615. https://doi.org/10.5006/1.3277591
7. J.M. George and S.S. Murthy, Influence of Generator Effectiveness on Performance of Vapour Absorption Heat Transformers, *Int. J. Energy Res.*, 1989, **13**(6), p 687–699. https://doi.org/10.1002/er.4440130608
8. A. Valero-Gómez, A. Igual-Muñoz, and J. García-Antón, Corrosion and Galvanic Behavior of Copper and Copper-Brazed Joints in Heavy Brine Lithium Bromide Solutions, *Corrosion*, 2006, **62**(12), p 1117–1131. https://doi.org/10.5006/1.3278245
9. E.A. Abd El Meguid, and N.K. Awad, Electrochemical Pitting Corrosion Behaviour of α-Brass in LiBr Containing Solutions, *Corros. Sci.*, 2009, **51**(5), p 1134–1139. https://doi.org/10.1016/j.corsci.2009.02.019
10. E.A. Abd El Meguid, S.S. Abd El Rehim, S.A. Al Kiey. Inhibitory Effect of Cetyltrimethyl Ammonoium Bromide on the Corrosion of 904L Stainless Steel in LiBr Solution, *Corros. Eng. Sci. Technol.*, 2016, **51**, p 429. https://doi.org/10.1080/1478422X.2015.1131799
11. J. Olsson and M. Snis, Duplex — A New Generation of Stainless Steels for Desalination Plants, *Desalination*, 2007, **205**(1), p 104–113. https://doi.org/10.1016/j.desal.2006.02.051
12. N. Solomon and I. Solomon, Effect of Deformation-Induced Phase Transformation on AISI 316 Stainless Steel Corrosion Resistance, *Eng. Fail. Anal.*, 2017, **79**, p 865–875. https://doi.org/10.1016/j.engfailanal.2017.05.031
13. J.R. Davis, *Stainless Steels*, ASM International, Singapore, 1994
14. E.A. Abd El Meguid, and A.A. Abd El Latif, Electrochemical and SEM Study on Type 254 SMO Stainless Steel in Chloride Solutions, *Corros. Sci.*, 2004, **46**(10), p 2431–2444. https://doi.org/10.1016/j.corsci.2004.01.022
15. G. Zou, W. Shi, S. Xiang, X. Ji, G. Ma, and R.G. Ballinger, Corrosion Behavior of 904L Austenitic Stainless Steel in Hydrofluoric Acid, *RSC Adv.*, 2018, **8**(5), p 2811–2817. https://doi.org/10.1039/C7RA12453H
16. J. Wang, W. Shi, S. Xiang, and R.G. Ballinger, Study of the Corrosion Behaviour of Sensitized 904L Austenitic Stainless Steel in Cl-Solution, *Corros. Sci.*, 2021, **181**, p 109234. https://doi.org/10.1016/j.corsci.2020.109234
17. R. Jiang, G. Zou, W. Shi, Y. Liang, and S. Xiang, Corrosion Behavior of Plasma-Nitrided 904L Austenitic Stainless Steel in Hydrofluoric Acid, *J. Mater. Eng. Perform.*, 2019, **28**(3), p 1863–1872. https://doi.org/10.1007/s11665-019-03938-y
18. Y. Han, G. Qiao, J. Sun, and D. Zou, A Comparative Study on Constitutive Relationship of As-Cast 904L Austenitic Stainless Steel during Hot Deformation Based on Arrhenius-type and Artificial Neural Network Models, *Comput. Mater. Sci.*, 2013, **67**, p 93–103. https://doi.org/10.1016/j.commatsci.2012.07.028
19. S. Pradhan, P. Bhuyan, and S. Mandal, Influence of the Individual Microstructural Features on Pitting Corrosion in Type 304 Austenitic Stainless Steel, *Corros. Sci.*, 2019, **158**, p 108091.
20. M. Li, D. Zou, Y. Li, and L. Tong, Effect of Cooling Rate on Pitting Corrosion Behavior of 904L Austenitic Stainless Steel in a Simulated Flue Gas Desulfurization Solution, *Met. Mater. Int.*, 2022 https://doi.org/10.1007/s12540-022-01255-z
21. R.T. Loto and C.A. Loto, Comparative Assessment of the Pitting Corrosion Resistance and Passivation Behaviour of 439L Ferritic and 904L Austenitic Stainless Steels for Application in Extreme Process Environments, *J. Bio- Tribo-Corros.*, 2019, **5**(3), p 1–15.
22. M. Lindgren, E. Huttunen-Saarivirta, H. Peltola, J. Romu, T. Sarikka, H. Hänninen, and P. Pohjanne, Crevice corrosion of Stainless Steels 904L, 2205, and 2507 in High-Temperature Sulfuric Acid Solution Containing Chlorides: Influence of Metal Cations, *Corrosion*, 2018, **74**(2), p 225–240.
23. M. Lindgren, S. Siljander, R. Suihkonen, P. Pohjanne, and J. Vuorinen, Erosion–Corrosion Resistance of Various Stainless Steel Grades in High-Temperature Sulfuric Acid Solution, *Wear*, 2016, **364**, p 10–21.
24. T. Prosek, A. Iversen, C. Taxen, Low Temperature Stress Corrosion Cracking of Stainless Steels in the Atmosphere in Presence of Chloride Deposits, in *Corrosion* 2008. 2008, OnePetro
25. V. Raja, Stress Corrosion Cracking Behaviour of 904L SS and Type 317L SS Weld-Fusion Zones in Boiling Water Reactor Startup Condition (2010)
26. A. Tomio, M. Sagara, T. Doi, H. Amaya, N. Otsuka, and T. Kudo, Role of Alloyed Copper on Corrosion Resistance of Austenitic Stainless Steel in H_2S–Cl− Environment, *Corros. Sci.*, 2014, **81**, p 144–151. https://doi.org/10.1016/j.corsci.2013.12.013
27. D. Ye, J. Li, W. Jiang, J. Su, and K. Zhao, Effect of Cu Addition on Microstructure and Mechanical Properties of 15%Cr Super Martensitic Stainless Steel, *Mater. Des.*, 2012, **41**, p 16–22. https://doi.org/10.1016/j.matdes.2012.04.036
28. E.E. Oguzie, J. Li, Y. Liu, D. Chen, Y. Li, K. Yang, and F. Wang, The Effect of Cu Addition on the Electrochemical Corrosion and Passivation Behavior of Stainless Steels, *Electrochim. Acta*, 2010, **55**(17), p 5028–5035.
29. E.A. Abd El Meguid, Pitting Susceptibility of UNS NO. 8904 Stainless Steel in Bromide-Sulphide Solution, *J. Mater. Sci.*, 1998, **33**(13), p 3465–3470. https://doi.org/10.1023/A:1013218320934
30. E.A. Abd El Meguid, and N.A. Mahmoud, Inhibition of Bromide-Pitting Corrosion of Type 904L Stainless Steel, *Corrosion*, 2003, **59**(2), p 104–111. https://doi.org/10.5006/1.3277539
31. A. Zambon, P. Ferro, and F. Bonollo, Microstructural, Compositional and Residual Stress Evaluation of CO_2 Laser Welded Superaustenitic AISI 904L Stainless Steel, *Mater. Sci. Eng., A*, 2006, **424**(1), p 117–127. https://doi.org/10.1016/j.msea.2006.03.003
32. N. Hakiki, M.D.C. Belo, A. Simoes, and M. Ferreira, Semiconducting Properties of Passive Films Formed on Stainless Steels: Influence of the Alloying Elements, *J. Electrochem. Soc.*, 1998, **145**(11), p 3821. https://doi.org/10.1149/1.1838880

33. R.M. Fernández-Domene, E. Blasco-Tamarit, D.M. García-García, and J. García-Antón, Effect of Alloying Elements on the Electronic Properties of Thin Passive Films Formed on Carbon Steel, Ferritic and Austenitic Stainless Steels in a Highly Concentrated LiBr Solution, *Thin Solid Films*, 2014, **558**, p 252–258. https://doi.org/10.1016/j.tsf.2014.03.042
34. A.K. Larios-Galvez, R. Lopez-Sesenes, E. Sarmiento-Bustos, I. Rosales, J. Uruchurtu-Chavarin, J. Porcayo-Calderon, and J.G. Gonzalez-Rodriguez, Corrosion Behavior of Steels in LiBr–H_2O–$CaCl_2$–$LiNO_3$ Systems, *Metals*, 2022, **12**(2), p 279. https://doi.org/10.3390/met12020279
35. G.Z. Meng, C. Zhang, and Y.F. Cheng, Effects of Corrosion Product Deposit on the Subsequent Cathodic and Anodic Reactions of X-70 Steel in Near-Neutral pH Solution, *Corros. Sci.*, 2008, **50**(11), p 3116–3122. https://doi.org/10.1016/j.corsci.2008.08.026
36. D. García-García, E. Blasco-Tamarit, and J. Garcia-Anton, Effects of the Area of a Duplex Stainless Steel Exposed to Corrosion on the Cathodic and Anodic Reactions in a LiBr Solution under Static and Dynamic Conditions, *Int. J. Electrochem. Sci.*, 2011, **6**(5), p 1237–1249.
37. E. Blasco-Tamarit, A. Igual-Muñoz, J.G. Antón, and D. García-García, Effect of Temperature on the Corrosion Resistance and Pitting Behaviour of Alloy 31 in LiBr Solutions, *Corros. Sci.*, 2008, **50**(7), p 1848–1857. https://doi.org/10.1016/j.corsci.2008.03.016
38. R.M. Fernández-Domene, E. Blasco-Tamarit, D.M. García-García, and J. García-Antón, Cavitation Corrosion and Repassivation Kinetics of Titanium in a Heavy Brine LiBr Solution Evaluated by Using Electrochemical Techniques and Confocal Laser Scanning Microscopy, *Electrochim. Acta*, 2011, **58**(1), p 264–275. https://doi.org/10.1016/j.electacta.2011.09.034
39. A.P. Bond, Anodic Polarization Behavior of High-Purity 13 and 18% Cr Stainless Steels, *J. Electrochem. Soc.*, 1975, **120**, p 453. https://doi.org/10.1149/1.2134307
40. C-O. A. Olsson and D. Landolt, Passive Films on Stainless Steels—Chemistry, Structure and Growth, *Electrochim. Acta*, (2003), **48**, p 1093. https://doi.org/10.1016/S0013-4686(02)00841-1
41. M. Kaneko and H.S. Isaacs, Effects of Molybdenum on the Pitting of Ferritic- and Austenitic-Stainless Steels in Bromide and Chloride Solutions, *Corros. Sci.*, 2002, **44**(8), p 1825–1834. https://doi.org/10.1016/S0010-938X(02)00003-3
42. C.O.A. Olsson, and D. Landolt, Passive Films on Stainless Steels—Chemistry, Structure and Growth, *Electrochim. Acta*, 2003, **48**(9), p 1093–1104. https://doi.org/10.1016/S0013-4686(02)00841-1
43. E. Blasco-Tamarit, A. Igual-Muñoz, J. García Antón, and D. García-García, Effect of Aqueous LiBr Solutions on the Corrosion Resistance and Galvanic Corrosion of an Austenitic Stainless Steel in its Welded and Non-Welded Condition, *Corros. Sci.*, 2006, **48**(4), p 863–886. https://doi.org/10.1016/j.corsci.2005.02.028
44. G.C. Palit, V. Kain, and H.S. Gadiyar, Electrochemical Investigations of Pitting Corrosion in Nitrogen-Bearing Type 316N Stainless Steel, *Corrosion*, 1993, **49**(12), p 979–991.
45. R.F.A. Jargelius-Pettersson, Electrochemical Investigation of the Influence of Nitrogen Alloying on Pitting Corrosion of Austenitic Stainless Steels, *Corros. Sci.*, 1999, **41**(8), p 1639–1664. https://doi.org/10.1016/S0010-938X(99)00013-X
46. R.C. Newman, W. R Whitney Award Lecture: Understanding the Corrosion of Stainless Steel, *Corrosion*, 2001, **57**(12), p 1030–1041. https://doi.org/10.5006/1.3281676
47. S.A.M. Refaey, Inhibition of Steel Pitting Corrosion in HCl by Some Inorganic Anions, *Appl. Surf. Sci.*, 2005, **240**(1), p 396–404. https://doi.org/10.1016/j.apsusc.2004.07.014
48. D.D. Macdonald, The Point Defect Model for the Passive State, *J. Electrochem. Soc.*, 1992, **139**(12), p 3434–3449. https://doi.org/10.1149/1.2069096
49. F. Herbert, A. Krishnamoorthy, W. Ma, K. Van Vliet, and B. Yildiz, Dynamics of Point Defect Formation, Clustering and Pit Initiation on the Pyrite Surface, *Electrochim. Acta*, 2014, **127**, p 416–426. https://doi.org/10.1016/j.electacta.2014.02.048
50. R. Case, Evaluation of the Passivity Limits in Austenitic Stainless Steel Exposed to H_2S-Containing Brines Using Point Defect Model Analysis, *Corros. Eng., Sci. Technol.*, 2022, **57**(2), p 118–131. https://doi.org/10.1080/1478422X.2021.1998952
51. C.Y. Chao, L.F. Lin, and D.D. Macdonald, A Point Defect Model for Anodic Passive Films I. Film Growth Kinetics, *J. Electrochem. Soc.*, 1981, **128**(6), p 1187–1194. https://doi.org/10.1149/1.2127591
52. Z. Szklarska-Smialowska, *Pitting Corrosion of Metals*, National Association of Corrosion Engineers, 1440 South Creep Drive, Houston Texas, USA, 1986
53. R. Leiva-García, M.J. Muñoz-Portero, and J. García-Antón, Corrosion Behaviour of Sensitized and Unsensitized Alloy 900 (UNS 1.4462) in Concentrated Aqueous Lithium Bromide Solutions at Different Temperatures, *Corros. Sci.*, 2010, **52**(3), p 950–959. https://doi.org/10.1016/j.corsci.2009.11.018
54. Z. Szklarska-Smialowska, Review of Literature on Pitting Corrosion Published Since 1960, *Corrosion*, 2013, **27**(6), p 223–233. https://doi.org/10.5006/0010-9312-27.6.223
55. J. Wang, C. Su, and Z. Szklarska-Smialowska, Effects of Cl− Concentration and Temperature on Pitting of AISI 304 Stainless Steel, *Corrosion*, 1988, **44**(10), p 732–737.
56. P.E. Manning and J. Duquette, The Effect of Temperature (25°–289°C) on Pit Initiation in Single Phase and Duplex 304L Stainless Steels in 100 ppm Cl− Solution, *Corros. Sci.*, 1980, **20**(4), p 597–609. https://doi.org/10.1016/0010-938X(80)90074-8
57. M.A. Amin, S.S. Abd El-Rehim, E.E.F. El-Sherbini, S.R. Mahmoud, and M.N. Abbas, Pitting Corrosion Studies on Al and Al–Zn Alloys in SCN− Solutions, *Electrochim. Acta*, 2009, **54**(18), p 4288–4296. https://doi.org/10.1016/j.electacta.2009.02.076
58. M.A. Ameer, A.M. Fekry, and F.E.-T. Heakal, Electrochemical Behaviour of Passive Films on Molybdenum-Containing Austenitic Stainless Steels in Aqueous Solutions, *Electrochim. Acta*, 2004, **50**(1), p 43–49. https://doi.org/10.1016/j.electacta.2004.07.011
59. M.S. Hasanin and S.A. Al Kiey, Environmentally Benign Corrosion Inhibitors Based on Cellulose Niacin Nano-Composite for Corrosion of Copper in Sodium Chloride Solutions, *Int. J. Biol. Macromol.*, 2020, **161**, p 345–354. https://doi.org/10.1016/j.ijbiomac.2020.06.04
60. S.A. Al Kiey, M.S. Hasanin, and S. Dacrory, Potential Anticorrosive Performance of Green and Sustainable Inhibitor Based on Cellulose Derivatives for Carbon Steel, *J. Mol. Liq.*, 2021, **338**, p 116604. https://doi.org/10.1016/j.molliq.2021.116604
61. S.A. Al Kiey, H.R.M. Rashdan, M.E. El-Naggar, Insight into Mitigation of Corrosion Behavior of Novel Chalcone Derivative for AZ91 Mg Alloy in Saline Solution: Synthesis, Characterization, Electrochemical and Adsorption Studies. *J. Electroanal. Chem.*, 2023, **934**, p 117304. https://doi.org/10.1016/j.jelechem.2023.117304
62. M. Hasanin and S.A. Al Kiey, Development of Ecofriendly High Performance Anti-Corrosive Chitosan Nanocomposite Material for Mild Steel Corrosion in Acid Medium, *Biomass Convers. Biorefinery*, 2021 https://doi.org/10.1007/s13399-021-02059-8
63. M.G.S. Ferreira, Electrochemical Studies of the Passive Film on 316 Stainless Steel in Chloride Media, *J. Electrochem. Soc.*, 1985, **132**(4), p 760–765. https://doi.org/10.1149/1.2113954
64. S.A. Al Kiey, M.S. Hasanin, F.E.-T. Heakal, Green and sustainable chitosan–gum Arabic nanocomposites as efficient anticorrosive coatings for mild steel in saline media, *Sci. Rep.*, 2022, **12**, p 13209. https://doi.org/10.1038/s41598-022-17386-7
65. P. Girault, J.L. Grosseau-Poussard, J.F. Dinhut, and L. Marechal, Influence of a Chromium Ion Implantation on the Passive Behaviour of Nickel in Artificial Sea-Water: An EIS and XPS Study, *Nucl. Instrum. Methods Phys. Res., Sect. B*, 2001, **174**(4), p 439–452. https://doi.org/10.1016/S0168-583X(00)00686-8
66. V. Vivier and M.E. Orazem, Impedance Analysis of Electrochemical Systems, *Chem. Rev.*, 2022, **122**(12), p 11131–11168.
67. A. Popova, E. Sokolova, S. Raicheva, and M. Christov, AC and DC Study of the Temperature Effect on Mild Steel Corrosion in Acid Media in the Presence of Benzimidazole Derivatives, *Corros. Sci.*, 2003, **45**(1), p 33–58.
68. A. Igual Muñoz, J. García Antón, J.L. Guiñón, and V. Pérez Herranz, The Effect of Chromate in the Corrosion Behavior of Duplex Stainless Steel in LiBr Solutions, *Corros. Sci.*, 2006, **48**(12), p 4127–4151. https://doi.org/10.1016/j.corsci.2006.03.009